The Plant Cell, Vol. 18, 715–730, March 2006, www.plantcell.org © 2006 American Society of Plant Biologists

Vacuolar H^+-ATPase Activity Is Required for Endocytic and Secretory Trafficking in *Arabidopsis* [W]

Jan Dettmer,[a] Anne Hong-Hermesdorf,[a] York-Dieter Stierhof,[b] and Karin Schumacher[a,1]

[a] Center for Plant Molecular Biology–Plant Physiology, Universität Tübingen, 72076 Tübingen, Germany
[b] Center for Plant Molecular Biology–Microscopy, Universität Tübingen, 72076 Tübingen, Germany

In eukaryotic cells, compartments of the highly dynamic endomembrane system are acidified to varying degrees by the activity of vacuolar H^+-ATPases (V-ATPases). In the *Arabidopsis thaliana* genome, most V-ATPase subunits are encoded by small gene families, thus offering potential for a multitude of enzyme complexes with different kinetic properties and localizations. We have determined the subcellular localization of the three *Arabidopsis* isoforms of the membrane-integral V-ATPase subunit VHA-a. Colocalization experiments as well as immunogold labeling showed that VHA-a1 is preferentially found in the *trans*-Golgi network (TGN), the main sorting compartment of the secretory pathway. Uptake experiments with the endocytic tracer FM4-64 revealed rapid colocalization with VHA-a1, indicating that the TGN may act as an early endosomal compartment. Concanamycin A, a specific V-ATPase inhibitor, blocks the endocytic transport of FM4-64 to the tonoplast, causes the accumulation of FM4-64 together with newly synthesized plasma membrane proteins, and interferes with the formation of brefeldin A compartments. Furthermore, nascent cell plates are rapidly stained by FM4-64, indicating that endocytosed material is redirected into the secretory flow after reaching the TGN. Together, our results suggest the convergence of the early endocytic and secretory trafficking pathways in the TGN.

INTRODUCTION

Organelles along the endocytic and secretory pathways have characteristic luminal pH values suited to their biochemical functions. The maintenance and regulation of these acidic microenvironments is achieved by the activity of vacuolar H^+-ATPases (V-ATPases), a class of primary electrogenic proton pumps found in all eukaryotes. V-ATPases are multisubunit enzyme complexes composed of the cytosolic ATP-hydrolyzing V_1 subcomplex (subunits A to H) and the membrane-bound proton-translocating V_0 subcomplex (subunits a, c, c′, c″, d, and e) (Nishi and Forgac, 2002; Nelson, 2003).

In plants, the most prominent role of the V-ATPase is to maintain ion and metabolite homeostasis by energizing secondary active transport across the tonoplast (Sze et al., 1999; Kluge et al., 2003). Although V-ATPases have also been found throughout the endomembrane system, including the endoplasmic reticulum, Golgi, and provacuoles (Chanson and Taiz, 1985; Ali and Akazawa, 1986; Herman et al., 1994; Oberbeck et al., 1994), the functions of the plant V-ATPase in secretory and endocytic trafficking are not well defined. In tobacco (*Nicotiana tabacum*) cells, inhibition of the V-ATPase interferes with secretion and leads to missorting of vacuolar proteins, suggesting that the functionality of a nonvacuolar compartment depends on V-ATPase function (Matsuoka et al., 1997). Analysis of V-ATPase null mutants of *Arabidopsis thaliana* has recently shown that the V-ATPase is essential for Golgi function during the development of the male gametophyte and during embryogenesis (Dettmer et al., 2005; Strompen et al., 2005). Therefore, it seems possible that the growth inhibition observed in plants with reduced V-ATPase activity (Schumacher et al., 1999; Padmanaban et al., 2004) is caused by a defect in vesicle trafficking rather than by reduced turgor pressure attributable to a lack of osmolyte transport into the vacuole.

In *Arabidopsis*, as in many higher eukaryotes, most subunits are encoded by small gene families (Sze et al., 2002), thus offering an enormous potential for different V-ATPase isoforms. The choice of subunits may determine not only the intrinsic activity of the pump or its ability to respond to regulatory signals but also its targeting to different intracellular locations. In yeast, subunit a is the only subunit encoded by two genes, *VPH1* (for *Vacuolar acidification–defective1*) and *STV1* (for *Similar to VPH1*) (Manolson et al., 1992, 1994). Whereas Vph1p resides at the tonoplast, Stv1p cycles continuously between a late Golgi compartment and prevacuolar endosomes (Manolson et al., 1994; Kawasaki-Nishi et al., 2001a). The membrane-integral subunit a consists of a hydrophilic N-terminal domain and a hydrophobic C-terminal domain with several predicted membrane-spanning domains (Manolson et al., 1992; Leng et al., 1999). Whereas the cytosolic N-terminal domain interacts with several subunits of the V_1 subcomplex and might be part of the peripheral stator (Landolt-Marticorena et al., 2000), the C-terminal domain is involved in proton translocation and assembly of the V-ATPase complex (Leng et al., 1998; Kawasaki-Nishi et al., 2001b).

A dynamic equilibrium between the fully assembled V-ATPase complex and the free subcomplexes V_1 and V_0 exists in many organisms and is known to be regulated by extracellular conditions in yeast and insects (Kane, 2000). Interestingly, it has been

[1] To whom correspondence should be addressed. E-mail karin.schumacher@uni-tuebingen.de; fax 49-7071-293287.
The author responsible for distribution of materials integral to the findings presented in this article in accordance with the policy described in the Instructions for Authors (www.plantcell.org) is: Karin Schumacher (karin.schumacher@uni-tuebingen.de).
[W] Online version contains Web-only data.
Article, publication date, and citation information can be found at www.plantcell.org/cgi/doi/10.1105/tpc.105.037978.

shown that the dissociation of V-ATPase complexes in response to glucose withdrawal differs between Vph1p-containing complexes at the vacuole and Stv1p-containing complexes at the late Golgi/early endosome (Kawasaki-Nishi et al., 2001c). Moreover, recent work has established precedence for acidification-independent functions of the V_0 subcomplex during homotypic vacuole fusion in yeast (Peters et al., 2001; Bayer et al., 2003) and synaptic vesicle fusion in *Drosophila* (Hiesinger et al., 2005). Although the presence of free V_1 and V_0 complexes has been demonstrated in plants (Li and Sze, 1999), it remains to be determined how V_1V_0 assembly is regulated and whether V_0 has functions independent of acidification in plants. To address these questions, it is first necessary to better understand the function of subunit a in plants and to gain insight into the roles of its isoforms.

Pharmacological studies using the specific, membrane-permeable inhibitors bafilomycin A and concanamycin A (ConcA) have established that V-ATPase activity is crucial for many aspects of the mammalian secretory and endocytic pathways, including the dissociation of receptor–ligand complexes (Forgac, 1999), the recruitment of proteins involved in vesicle formation (Aniento et al., 1996; Maranda et al., 2001), and transport between different endosomal compartments (Clague et al., 1994; van Weert et al., 1995; Tawfeek and Abou-Samra, 2004). Genetic evidence supports the results obtained with V-ATPase inhibitors: in *vph1*Δ/*stv1*Δ and other V-ATPase null mutants of yeast, transport of the endocytic tracer FM4-64 to the vacuole is delayed (Perzov et al., 2002; Iwaki et al., 2004), and reduced expression of the *Dictyostelium* gene encoding subunit a slowed phagocytosis and prolonged endosomal transit time (Liu et al., 2002).

Endocytic cycling of plasma membrane proteins has been shown to be important for plant cell polarity and behavior (Geldner et al., 2003; Meckel et al., 2004). However, structural and operational descriptions of plant endosomal compartments still need to be reconciled (Geldner, 2004; Samaj et al., 2005), and the role of the V-ATPase in endocytic trafficking in plants is largely unaddressed.

To determine whether organelle-specific V-ATPase isoforms exist in higher plants and to gain further insight into the functions of the *Arabidopsis* V-ATPase in the endocytic and secretory pathways, we analyzed the subcellular localization of the three *Arabidopsis* isoforms of subunit a (VHA-a). Here, we provide evidence that VHA-a1 is localized in an early endosomal compartment, which we identified by immunogold labeling as well as by colocalization experiments as the *trans*-Golgi network (TGN). Our analysis shows that ConcA leads to the accumulation of endocytosed material together with newly synthesized plasma membrane proteins, suggesting that, in *Arabidopsis*, trafficking pathways to and from the plasma membrane converge in the TGN.

RESULTS

Arabidopsis VHA-a Isoforms Are Differentially Localized

To determine the subcellular localization of the three *Arabidopsis* VHA-a isoforms VHA-a1 (At2g28520), VHA-a2 (At2g21410), and VHA-a3 (At4g39080), we constructed translational fusions between their genomic sequences and the reporter gene green fluorescent protein (GFP). The genomic DNA fragments included promoter regions of 1.3 kb (VHA-a1), 3.2 kb (VHA-a2), and 4.1 kb (VHA-a3), and GFP was fused to the last exon. Based on the prediction of six transmembrane-spanning domains for all *Arabidopsis* VHA-a isoforms (Schwacke et al., 2003), a cytosolic location of GFP is assumed. Homozygous lines with a single T-DNA insertion site were established, and RT-PCR was used to identify lines in which the expression level of the transgene was comparable to that of the endogenous gene (see Supplemental Figure 1A online). Furthermore, we performed coimmunoprecipitations of VHA-a1–GFP and VHA-A to demonstrate that at least a substantial fraction of V-ATPase complexes contain VHA-a1–GFP (see Supplemental Figure 1B online). The fact that VHA-a1–GFP is integrated into the V-ATPase holocomplex suggests that it is functional, because the integration of a nonfunctional subunit into the complex likely would have had dominant negative effects. However, all lines expressing VHA-a1–GFP were indistinguishable from the wild type.

In seedlings, expression of the GFP fusion proteins was detectable in all cells (see Supplemental Figure 2 online), and their localization in cells of the root elongation zone was examined by confocal laser scanning microscopy (CLSM). A mobile, punctate staining pattern was observed in seedlings of all lines expressing VHA-a1–GFP (Figure 1A), whereas seedlings expressing VHA-a2–GFP (Figure 1B) or VHA-a3–GFP (see Supplemental Figure 2L online) displayed fluorescence preferentially at the tonoplast. To exclude the possibility that the observed localization of VHA-a1 was an artifact caused by the fusion of GFP to its C terminus, we constructed a chimeric protein consisting of the N-terminal part of VHA-a1 (amino acids 1 to 228) and the C terminus of VHA-a2 (amino acids 233 to 820) fused to GFP. In transgenic seedlings expressing VHA-a1a2–GFP, a similar pattern as for VHA-a1–GFP was observed (Figure 1C); therefore, we assume that the C-terminal GFP fusion does not cause the mislocalization of VHA-a1. This result further indicates that the first 228 amino acids of the cytosolic N-terminal domain contain the targeting information necessary for the specific localization of VHA-a1.

VHA-a1–GFP Is Localized in the TGN

The fungal toxin brefeldin A (BFA) inhibits certain ADP-ribosylation factor–guanine-nucleotide exchange factors (ARF-GEFs) and is widely used as a vesicle trafficking inhibitor (Peyroche et al., 1999; Robineau et al., 2000; Nebenfuhr et al., 2002). After BFA treatment, both VHA-a1–GFP and VHA-a1a2–GFP signals rapidly aggregated and were found throughout the vesicle agglomerations known as BFA compartments (Figures 1D and 1F) together with the endocytic tracer FM4-64 (Figure 1E). Early endosomal compartments accumulate in the core of BFA compartments (Geldner et al., 2001), whereas *trans*-Golgi markers tend to be found more in the periphery of BFA compartments (Wee et al., 1998; Grebe et al., 2003). The presence of VHA-a1–GFP in BFA compartments suggests that it is localized either in endosomes or in a *trans*-Golgi compartment; therefore, we performed colocalization experiments with appropriate marker proteins fused to monomeric red fluorescent protein (mRFP) (Campbell et al., 2002). In *Arabidopsis*, the plant-unique Rab5 homolog ARA6 and the Rab5 homolog ARA7 are localized on two distinct but partially overlapping

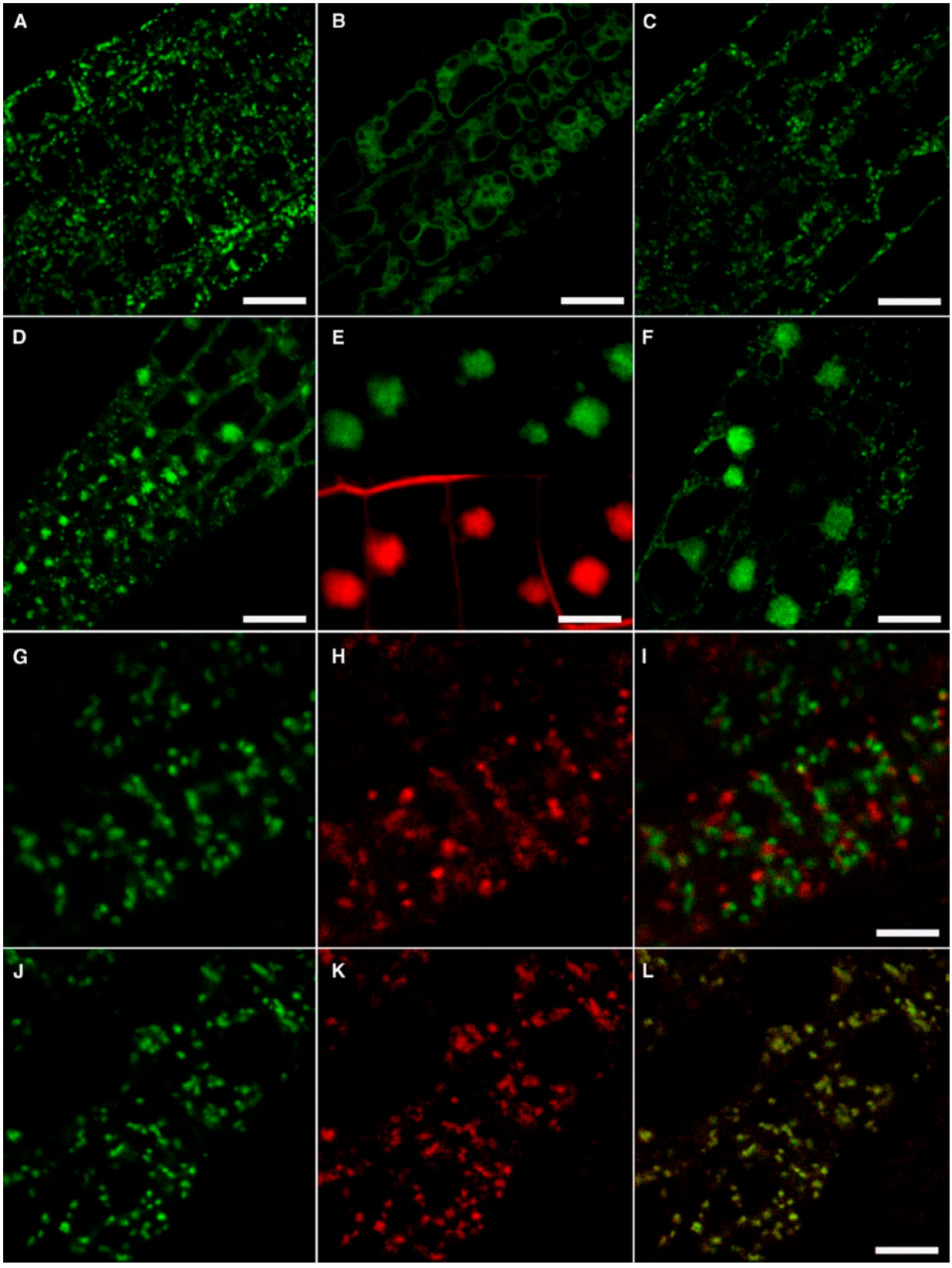

Figure 1. Subcellular Localization of VHA-a–GFP Fusion Proteins Expressed in Roots of Seedlings.

populations of endosomes (Ueda et al., 2001, 2004). In transgenic T1 seedlings coexpressing VHA-a1–GFP and ARA7-mRFP (Ueda et al., 2004), little overlap was detected (Figures 1G to 1I). Quantification of CLSM images revealed that <20% of the pixels with signal intensities above the chosen threshold overlapped between the red and green channels, and line scans confirmed that the intensity maxima did not colocalize (see Supplemental Figure 4A online). SYP41 (Tlg2a) is a member of the Qa SNARE group localized at the TGN in a complex with At VTI12, At VPS45, and SYP61 (Bassham et al., 2000; Sanderfoot et al., 2001). A fusion of SYP41 with GFP colocalizes with SYP61 but not with Golgi and prevacuolar compartment markers (Uemura et al., 2004). SYP41-mRFP had not been described previously; therefore, we confirmed that it showed the same localization as SYP41-GFP in transiently expressing protoplasts (see Supplemental Figures 3A to 3C online), indicating that the presence of mRFP did not affect the targeting of SYP41. In transgenic T1 seedlings coexpressing VHA-a1–GFP and SYP41-mRFP (Figures 1J to 1L), the punctate staining patterns were almost identical, indicating colocalization of the two proteins. Quantification of CLSM images revealed that >80% of the pixels with signal intensities above the chosen threshold overlapped between the red and green channels, and line scans confirmed that the intensity maxima did colocalize (see Supplemental Figure 4B online).

Immunogold electron microscopy was performed to confirm the colocalization results. In ultrathin cryosections of root tissue from VHA-a1–GFP seedlings incubated with a GFP antibody, gold particles specifically labeled tubulovesicular membranes in the vicinity of the *trans* site of Golgi stacks (Figures 2A, 2D, 2E, and 2G) that we interpret to be the TGN. Both the density of gold particles and their distance from the Golgi stack showed some variation; however, ultrastructural analysis (Figures 2C and 2F) showed that the extension of the TGN and its position relative to the Golgi stack are similarly variable. Labeling of the TGN was observed in seedlings in which transgene expression matched the level of the endogenous gene and in seedlings that overexpressed VHA-a1–GFP. Unfortunately, colabeling with a SYP41 antibody (Bassham et al., 2000) was not possible because of a lack of specific SYP41 signals. Labeling of the TGN was also observed in cells expressing the chimeric VHA-a1a2–GFP (Figure 2I), confirming that the targeting information resides in the N-terminal domain of VHA-a1. In cells expressing the *trans*-Golgi marker N-ST-YFP (Grebe et al., 2003), gold particles were located at the *trans*-most Golgi cisternae (Figure 2J) and in cells with high expression levels, also often in the TGN. No labeling above background was detected in wild-type cells (Figure 2L).

To provide further evidence that the observed localization of VHA-a1–GFP reflects the localization of the endogenous protein, we analyzed the distribution of the V-ATPase in wild-type root cells. Immunogold labeling using an antibody against VHA-E (Betz and Dietz, 1991) resulted in the expected labeling of the tonoplast (Figure 2B), but labeling in the TGN was also observed (Figure 2H). In *tuff* embryos lacking VHA-E1 (Strompen et al., 2005), the VHA-E antibody did not yield staining above background, thus confirming the specificity of the observed signals at the TGN and the tonoplast (Figure 2M).

Our results show that, in *Arabidopsis* root cells, the TGN and the tonoplast are the endomembranes with the highest V-ATPase density and provide evidence that VHA-a1–GFP reflects the preferential localization of the endogenous protein in the TGN.

Rapid Colocalization of VHA-a1–GFP with FM4-64

After BFA treatment, VHA-a1–GFP was found to colocalize with FM4-64, raising the possibility that it resides in an endosomal compartment. Although concerns have been raised (Bolte et al., 2004), FM4-64 is now widely accepted as a reliable tracer for endocytic trafficking (Geldner et al., 2003; Grebe et al., 2003; Meckel et al., 2004; Samaj et al., 2005); therefore, we used FM4-64 to determine the position of VHA-a1–GFP in the endocytic pathway.

The uptake of FM4-64 into *Arabidopsis* root tip cells can be blocked either by cold pretreatment or by treatment with wortmannin (data not shown); thus, it can be assumed that FM4-64 is internalized exclusively via endocytosis and follows the endocytic pathway from the plasma membrane to the tonoplast. Colocalization of FM4-64 and GFP was observed in root cells expressing VHA-a1–GFP after uptake for 6 min (Figures 3A to 3C; see Supplemental Figure 4C online). In fact, the first detectable intracellular FM4-64 fluorescence observed after only 2 min coincided with VHA-a1–GFP-labeled compartments. In agreement with this observation, the first intracellular FM4-64 fluorescence was often found adjacent to or overlapping with N-ST-YFP signals (Figures 3D to 3F). Uptake experiments were also performed with T1 seedlings expressing ARA6-GFP (Grebe et al., 2003) or ARA7-GFP (Ueda et al., 2001). No colocalization of FM4-64 with ARA7-GFP (Figures 3G to 3I) or ARA6-GFP (Figures 3J to 3L) was observed after 6 min. After 15 min, partial overlap was detected with ARA7-GFP but not with ARA6-GFP (data not shown). Together, these results indicate that VHA-a1–GFP resides in an early endosomal compartment distinct from the endosomes marked by either ARA6-GFP or ARA7-GFP.

ConcA Affects Endocytic Trafficking

The results presented to this point suggest that VHA-a1–GFP labels a compartment that may be part of both the endocytic and

Figure 1. (continued).

(A) to **(C)** Cells in the root elongation zone expressing VHA-a1–GFP **(A)**, VHA-a2–GFP **(B)**, and VHA-a1a2–GFP **(C)**. Bars = 25 μm.
(D) to **(F)** Cells expressing VHA-a1–GFP (**[D]** and **[E]**) and VHA-a1a2–GFP **(F)** after treatment with BFA for 1 h. Costaining with FM4-64 is shown in **(E)**. Bars = 25 μm (**[D]** and **[F]**) and 10 μm **(E)**.
(G) to **(I)** Cells coexpressing VHA-a1–GFP and the endosome marker ARA7-mRFP. Shown are the GFP channel (green **[G]**), the separately recorded mRFP channel (red **[H]**), and the overlay **(I)**. Bar = 10 μm.
(J) to **(L)** Cells coexpressing VHA-a1–GFP and the TGN marker SYP41-mRFP. Shown are the GFP channel (green **[J]**), the separately recorded mRFP channel (red **[K]**), and the overlay **(L)**. Bar = 10 μm.

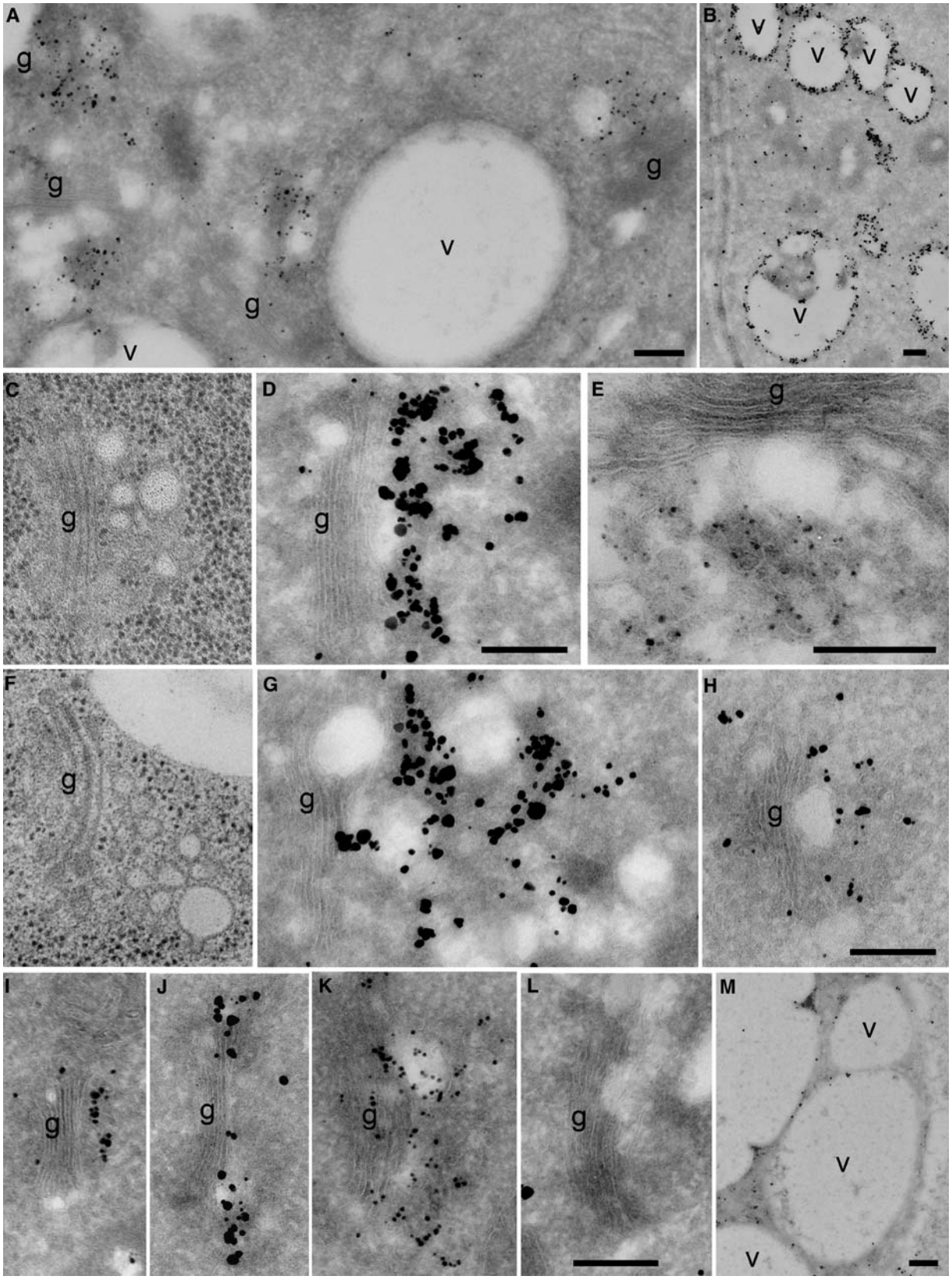

Figure 2. Immunogold Localization of VHA-a1–GFP and TGN Morphology.

the secretory pathways. To determine whether V-ATPase activity is necessary for the biological functions of this compartment, we next analyzed the effects of the V-ATPase inhibitor ConcA (Drose et al., 1993; Huss et al., 2002) on endocytic trafficking. To determine whether ConcA blocks the transport of FM4-64 to the tonoplast, we first analyzed the time course of FM4-64 trafficking in untreated root tip cells. After 1 h, FM4-64 staining distinct from that of the VHA-a1–GFP-labeled compartment was observed (Figures 4A to 4C), which can be interpreted as a later endosomal compartment through which the dye has to pass on its way to the tonoplast. Staining of the tonoplast was clearly detectable after 2 h (Figures 4D to 4F). Pretreatment with ConcA for 1 h and subsequent staining with FM4-64 revealed that the internalization of the dye is at least not strongly affected. However, after 2 h, neither FM4-64 signals clearly distinct from VHA-a1–GFP nor staining of the tonoplast was observed (Figures 4G to 4I). Weak tonoplast staining was seen only after prolonged incubation (Figures 4J to 4L). Comparable results were obtained using *Arabidopsis* suspension cultured cells, which were either untreated or pretreated with ConcA for 1 h, stained with FM4-64 at 4°C for 30 min, and washed before incubation in inhibitor-free medium or in ConcA medium (see Supplemental Figure 5 online).

Based on the results that VHA-a1–GFP is localized in the first compartment stained after FM4-64 uptake and that ConcA interferes with transport from this compartment to the vacuole, we conclude that ConcA inhibits transport from an early to a later endosomal compartment.

ConcA Affects Golgi Morphology and Interferes with BFA Action

ConcA not only blocked FM4-64 transport, it also affected the appearance of the VHA-a1–GFP staining pattern. Compared with untreated cells, diffuse and enlarged intracellular fluorescence signals (Figures 4E and 4G) were observed. Ultrastructural images of high-pressure frozen and freeze-substituted ConcA-treated root cells showed changes in Golgi morphology and aggregations of swollen vesicles, as described previously for tobacco BY2 cells (Robinson et al., 2004) and lily (*Lillium longiflorum*) pollen tubes (Dettmer et al., 2005). The effects of ConcA include bending of Golgi cisternae, swelling of their ends (Figure 5A), fragmentation of Golgi stacks, and the accumulation of large vesicles (Figures 5B to 5D). Immunogold labeling using GFP antibodies confirmed the presence of VHA-a1–GFP in ConcA-induced vesicle aggregates, indicating that they are derived from the TGN (Figure 5G).

Having shown that V-ATPase activity is necessary for endocytic trafficking and that VHA-a1–GFP is present in BFA compartments, we next asked whether V-ATPase function is also necessary for the formation of BFA compartments. The ultrastructure of a typical BFA compartment is shown in Figure 5E, and immunogold labeling using GFP antibodies confirmed that VHA-a1–GFP is evenly distributed in BFA compartments (Figure 5H). When seedlings were pretreated with ConcA for 1 h before BFA treatment, the typical large BFA compartments were never observed by CLSM. Electron microscopy images show a mixture of ConcA-like (Figure 5F) and small BFA-like aggregations. The observed effects of BFA and ConcA on VHA-a1–GFP were reversible by incubation of seedlings without inhibitors for 3 h (data not shown). Together, these results show that the TGN is a core component of BFA compartments and that V-ATPase function is required for their formation.

Endocytic and Secretory Trafficking Merge in the TGN

The TGN is the main sorting station of the secretory pathway; therefore, ConcA should interfere not only with endocytic trafficking but also with secretory trafficking. Root cells of seedlings expressing the plasma membrane steroid receptor BRI1 (Friedrichsen et al., 2000; Kinoshita et al., 2005) fused to GFP show detectable intracellular fluorescence (Russinova et al., 2004). The majority of intracellular BRI1-GFP signals were costained with FM4-64 in <10 min (Figure 6B), suggesting that they could be derived from TGN-localized molecules. After ConcA treatment, many cells showed increased intracellular BRI1-GFP fluorescence in irregular patches (Figure 6C). The BRI1-GFP patches were only partly stained by FM4-64 (Figure 6D), suggesting that ConcA may cause the accumulation of BRI1-GFP not only in the TGN but also either in Golgi stacks, if

Figure 2. (continued).

Immunogold labeling of ultrathin cryosections was performed with anti-GFP antibodies (**[A]**, **[D]**, **[E]**, **[G]**, and **[I]** to **[L]**) or anti–VHA-E antibodies (**[B]**, **[H]**, and **[M]**) and silver-enhanced Nanogold IgG. In **(L)**, silver-enhanced Qdot525 IgG was used as a marker.

(A) Overview of an immunogold-labeled cryosection of a root tip cortex cell expressing VHA-a1–GFP. Gold markers accumulate in the vicinity of Golgi stacks (g).

(B) The anti–VHA-E antibody strongly labels vacuolar membranes (v) and, to a lesser extent, the TGN region (see **[H]**).

(C) and **(F)** Electron micrographs of Golgi stacks and their associated TGNs in high-pressure frozen and freeze-substituted root tip cortex cells, shown at the same magnification as **(D)**, **(G)**, and **(H)**.

(D), **(E)**, and **(G)** Golgi stacks and their associated TGNs after immunogold labeling of VHA-a1–GFP in root cortex cells.

(H) Labeling of wild-type cells using anti–VHA-E antibodies results in gold labeling in the vicinity of Golgi stacks and on vacuolar membranes (see **[B]**).

(I) The a1a2-GFP chimeric protein can be detected on the TGN.

(J) and **(K)** N-ST-GFP is located at the *trans*-most Golgi cisternae **(J)** and often also in the TGN **(K)**. Labeling of N-ST-GFP with the silver-enhanced Quantum dot marker (Qdot525) **(J)** resulted in a labeling pattern and label density similar to those of silver-enhanced Nanogold markers.

(L) Control labeling on wild-type root cryosections using anti-GFP antibodies and silver-enhanced Nanogold was negligible.

(M) Control labeling with anti–VHA-E antibodies on cryosections of a VHA-E1–deficient embryo (Strompen et al., 2005). There are only a few gold particles on vacuolar membranes.

Bars = 0.25 μm.

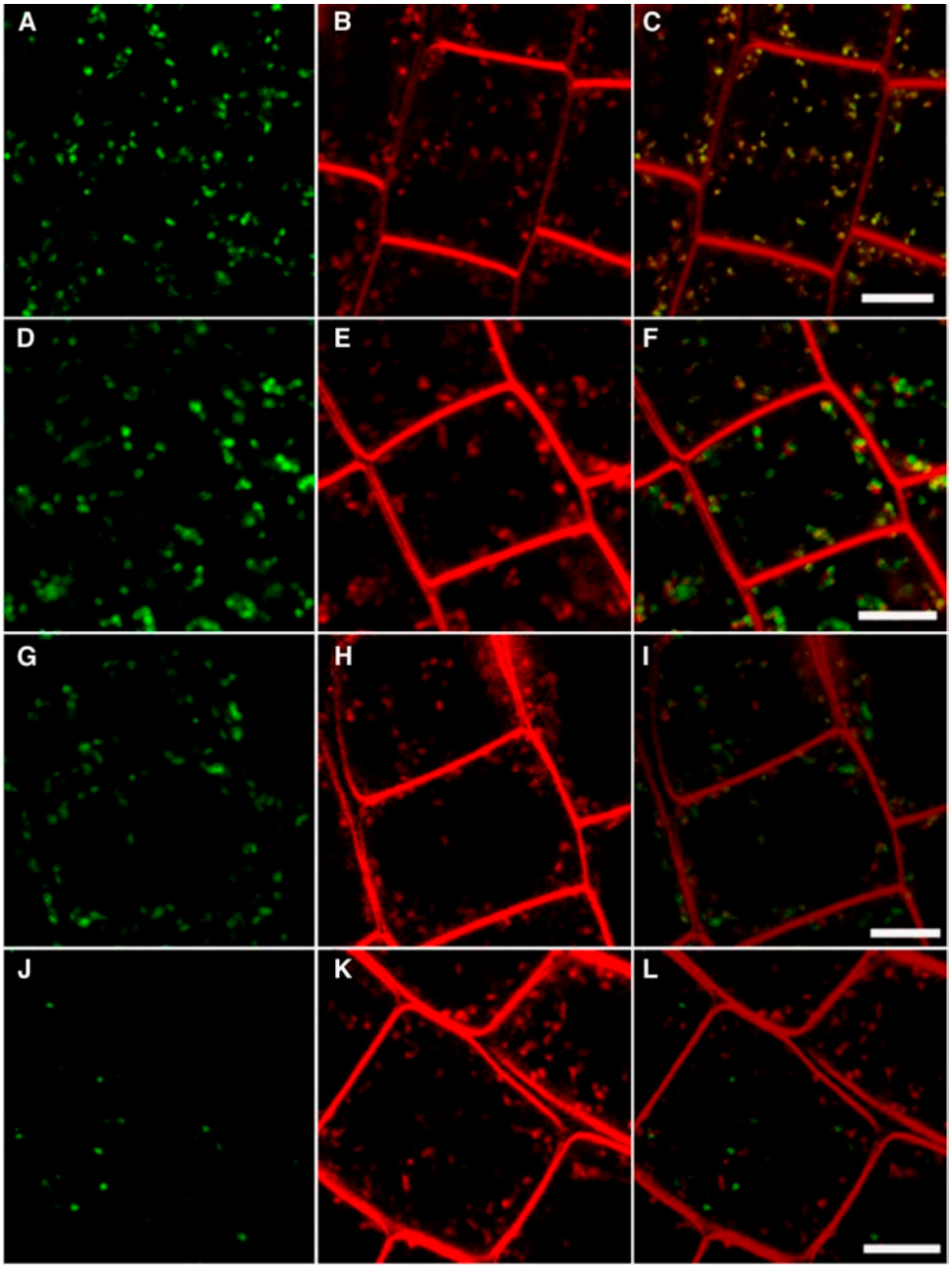

Figure 3. Rapid Colocalization of VHA-a1–GFP with FM4-64.

Cells in the root elongation zone expressing different GFP markers were stained with the endocytic tracer FM4-64: VHA-a1–GFP **(A)**, N-ST-YFP **(D)**, ARA7-GFP **(G)**, and ARA6-GFP **(J)**. Overlays of the separately recorded GFP (green) and FM4-64 (red) channels (**[B]**, **[E]**, **[H]**, and **[K]**) are shown in **(C)**, **(F)**, **(I)**, and **(L)**. All images were taken after 6 min of FM4-64 uptake. Bars = 10 μm.

ConcA causes the accumulation of newly synthesized plasma membrane proteins, or in a later endosomal compartment, if ConcA interferes with the recycling of internalized plasma membrane proteins. To determine whether the intracellular BRI1-GFP fluorescence was caused by internalized or newly synthesized molecules, protein synthesis was inhibited with cycloheximide (CHX). In both untreated (Figure 6E) and ConcA-treated (Figure 6G) seedlings, intracellular fluorescence was strongly reduced by CHX treatment, indicating that a substantial fraction of the intracellular BRI1-GFP signal is derived from secretory cargo. The intracellular signals remaining after CHX treatment did not show rapid colocalization with FM4-64 (Figures 6F and 6H), suggesting that they might be derived from later endosomal compartments. After ConcA treatment, these compartments

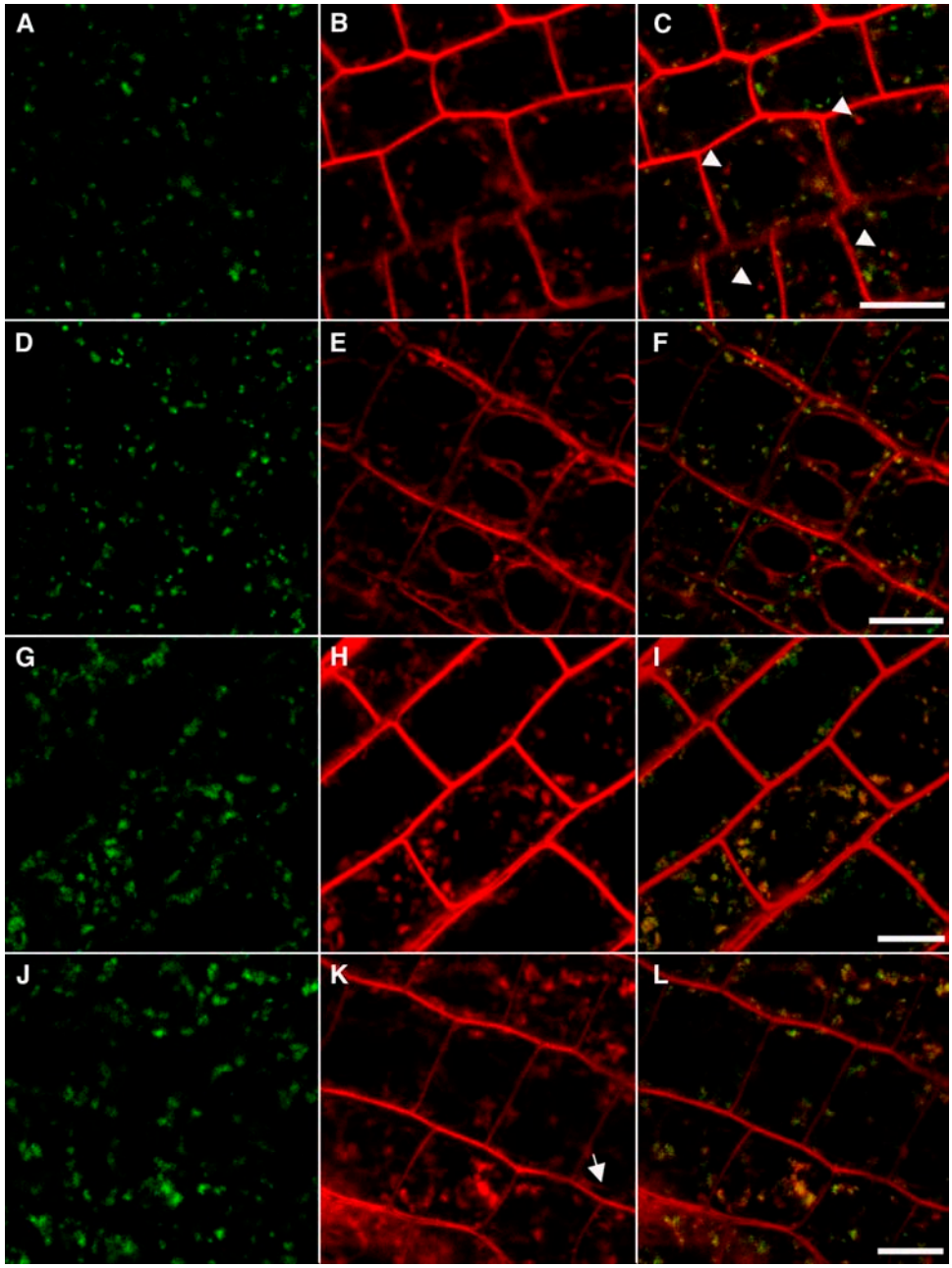

Figure 4. ConcA Blocks FM4-64 Transport to the Tonoplast.

Cells in the root elongation zone expressing VHA-a1–GFP were stained with the endocytic tracer FM4-64. Shown are the GFP channel (**[A]**, **[D]**, **[G]**, and **[J]**), the FM4-64 channel (**[B]**, **[E]**, **[H]**, and **[K]**), and overlays of the separately recorded GFP (green) and FM4-64 (red) channels (**[C]**, **[F]**, **[I]**, and **[L]**). Bars = 10 μm.

(A) to **(C)** Untreated cells expressing VHA-a1–GFP 1 h after FM4-64 staining. Arrowheads mark FM4-64 staining separate from VHA-a1–GFP signal that might represent later endosomal compartments.

(D) to **(F)** Untreated cells expressing VHA-a1–GFP 2 h after FM4-64 staining.

(G) to **(I)** ConcA-treated seedling root cells expressing VHA-a1–GFP 2 h after FM4-64 staining. Note the absence of FM4-64 staining not associated with VHA-a1–GFP and of tonoplast staining.

(J) to **(L)** ConcA-treated seedling root cells expressing VHA-a1–GFP 5 h after FM4-64 staining. The arrow indicates faint tonoplast staining.

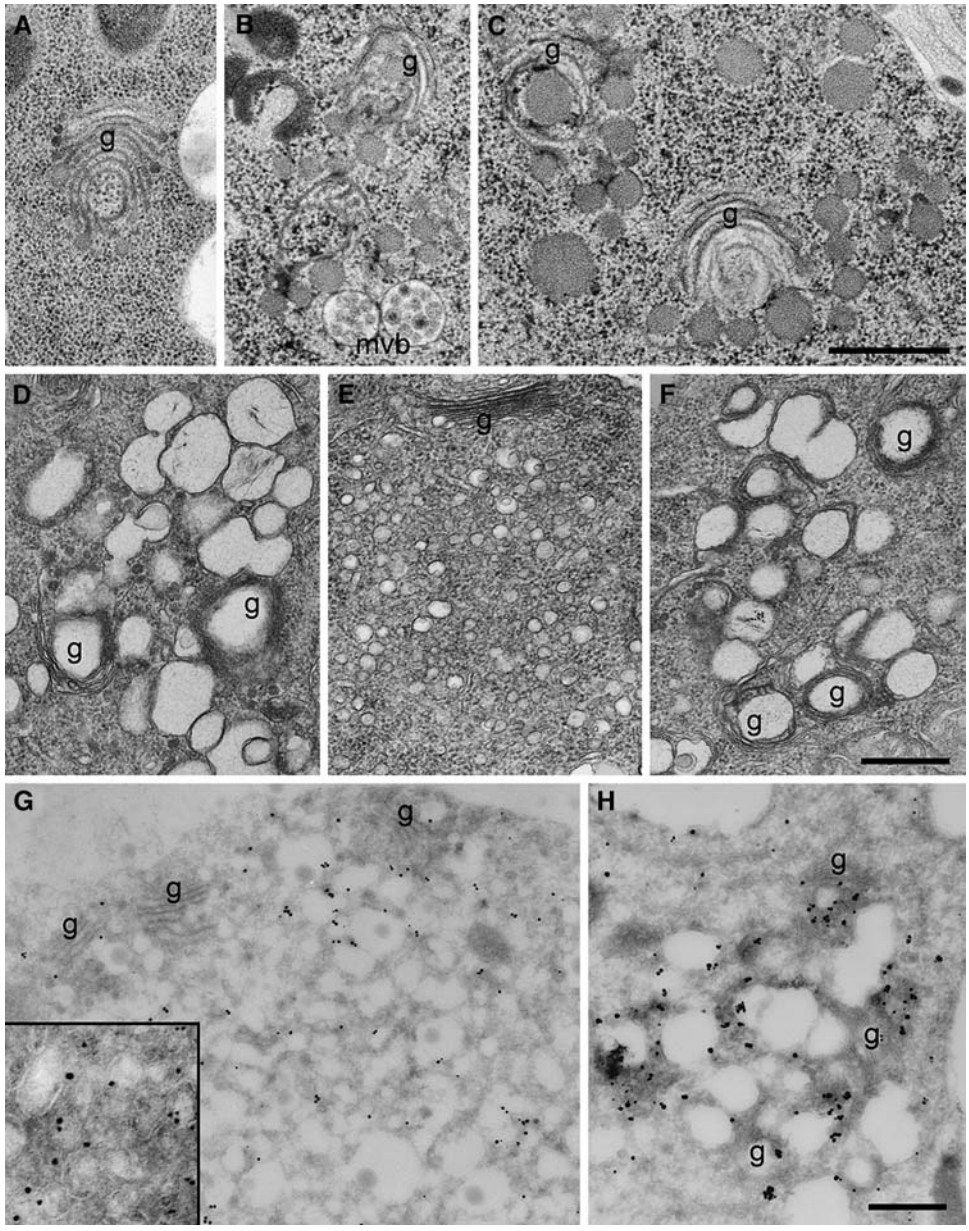

Figure 5. ConcA Induces Changes of TGN and Golgi Stack Morphology and Interferes with BFA Action.

(A) to **(C)** Electron micrographs of high-pressure frozen and freeze-substituted root tip cortex cells showing changes in Golgi and TGN morphology after ConcA treatment, such as the characteristic bending and swelling of the ends of cisternae **(A)** and the fragmentation of Golgi stacks and the accumulation of large vesicles (**[B]** and **[C]**). g, Golgi stack; mvb, multivesicular bodies.

(D) to **(F)** Electron micrographs of chemically fixed root tip cortex cells showing vesicle agglomerations induced by ConcA **(D)**, BFA **(E),** and ConcA followed by BFA **(F)**. The content of ConcA-induced vesicles is lost after chemical fixation and dehydration at ambient temperature (cf. **[C]**).

(G) and **(H)** Immunogold labeling of VHA-a1–GFP on cryosections of root tip cortex cells using anti-GFP antibodies and silver-enhanced Nanogold after ConcA treatment **(G)** and BFA treatment **(H)**. BFA and ConcA compartments are labeled. The inset in **(H)** shows a 2.5× enlarged detail of a thicker cryosection with gold-labeled vesicles of different sizes.

Bars = 0.5 μm.

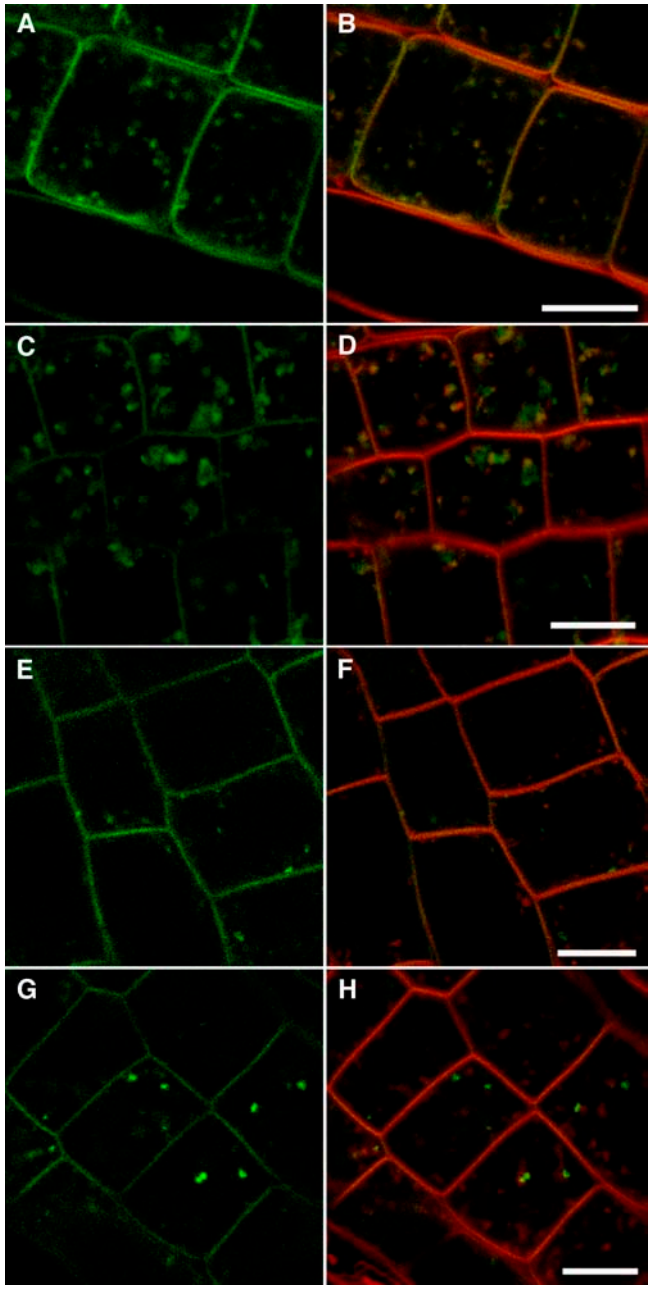

Figure 6. ConcA Induces Intracellular BRI1-GFP Accumulation.

Cells in the root elongation zone expressing BRI1-GFP were stained with the endocytic tracer FM4-64. Shown are the GFP channels (**[A]**, **[C]**, **[E]**, and **[G]**) and overlays of the separately recorded GFP (green) and FM4-64 (red) channels (**[B]**, **[D]**, **[F]**, and **[H]**). Bars = 10 μm.

(A) and **(B)** Untreated cells expressing BRI1-GFP stained with FM4-64 for 10 min.

(C) and **(D)** Cells expressing BRI1-GFP treated with ConcA for 2 h in the presence of FM4-64.

(E) and **(F)** Cells expressing BRI1-GFP treated with CHX for 1 h in the presence of FM4-64.

(G) and **(H)** Cells expressing BRI1-GFP treated with CHX for 1 h followed by treatment with ConcA + CHX for 1 h in the presence of FM4-64.

seem to be associated with but still separated from the FM4-64–stained membranes (Figure 6H). Our findings suggest that after ConcA treatment, secretory and endocytic cargos accumulate together in TGN-derived structures.

Nascent Cell Plates Are Rapidly Stained by FM4-64

Because it could be argued that the observed coaccumulation of endocytic and secretory cargos in the TGN is based on an artificial fusion of the TGN and endosomes caused by ConcA, we next addressed the question of whether early convergence of endocytic and secretory trafficking can be demonstrated in undisturbed cells. Transport to the plane of division is assumed to be the default pathway for Golgi-derived vesicles in dividing cells. It has been shown previously that FM4-64 enters the secretory pathway and stains cell plates in dividing *Fucus* and BY2 cells (Belanger and Quatrano, 2000; Bolte et al., 2004), but to date rapid entry into the secretory pathway has only been described in pollen tubes (Parton et al., 2001). Based on the results presented here, developing cell plates in *Arabidopsis* root tips should be rapidly stained by FM4-64 if the dye is redirected into the secretory vesicle flow after reaching the TGN. Indeed, in seedlings expressing VHA-a1–GFP, staining of cell plates was observed within 5 to 10 min after FM4-64 staining of the TGN was detected (Figure 7A). Three-dimensional reconstruction of Z

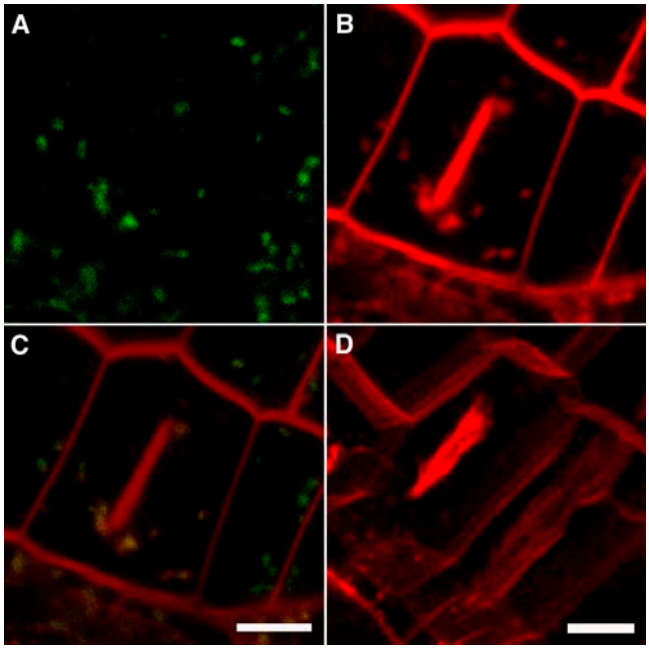

Figure 7. Nascent Cell Plates Are Rapidly Stained by FM4-64.

(A) to **(C)** Dividing cells expressing VHA-a1–GFP were stained with the endocytic tracer FM4-64. Images were taken within 15 min of FM4-64 staining. Shown are the separately recorded GFP **(A)** and FM4-64 **(B)** channels as well as the overlay **(C)**.

(D) Three-dimensional reconstruction of an image stack derived from a Z scan shows that the cell plate is not connected to the surrounding plasma membrane.

Bars = 5 μm.

scans showed that cell plates stained by FM4-64 were not yet connected with the cortical plasma membrane (Figure 7B). These findings strongly suggest that early endocytic and secretory trafficking converge in the TGN of *Arabidopsis* root tip cells.

DISCUSSION

Differential Localization of V-ATPase Isoforms in a Higher Plant

Organelle-specific isoforms of V-ATPase subunits have been best characterized in yeast, but specific sorting of isoforms of subunit a has also been reported in mouse osteoclasts (Toyomura et al., 2000) and in *Torpedo* neurons (Morel et al., 2003), in which specific isoforms are associated with the plasma membrane. We show here that organelle-specific distribution also exists in plants. As isoform-specific antibodies against VHA-a are not available, we used stable transgenic seedlings expressing GFP fusion proteins of the VHA-a isoforms to determine their subcellular localization. In contrast with the tonoplast-localized GFP fusion proteins of VHA-a2 and VHA-a3, VHA-a1 showed a distinct punctate staining pattern. GFP fusion proteins do not necessarily reflect the localization of the endogenous protein, as targeting signals might be obstructed by the presence of GFP or overexpression might interfere with correct targeting. Therefore, we used material in which the expression of VHA-a1 and VHA-a1–GFP was comparable and constructed a chimeric protein to demonstrate that the observed localization of VHA-a1 is caused neither by GFP nor by overexpression and to conclude that VHA-a1–GFP reflects the localization of the endogenous protein.

Colocalization as well as immunogold labeling experiments showed that VHA-a1–GFP was preferentially localized in the TGN, whereas VHA-a2–GFP and VHA-a3–GFP were detected at the tonoplast. None of the three *Arabidopsis* VHA-a isoforms showed a specific endoplasmic reticulum localization (Kluge et al., 2004). As in the case of Stv1p, the targeting information resides in the N-terminal cytosolic domain of VHA-a1; however, obvious sequence similarities that might reveal potential targeting signals do not exist, and it remains to be determined how the specific localization is achieved. Moreover, it has been shown in yeast that the isoforms confer different stability and different kinetic properties to the V-ATPase (Kawasaki-Nishi et al., 2001a), and it will be of interest to determine in which way complexes containing VHA-a1 are adapted to the requirements of the TGN. Interestingly, it has been shown that the V-ATPases found in Golgi- or tonoplast-enriched tobacco membrane fractions show different sensitivities to the V-ATPase inhibitors ConcA and bafilomycin A (Matsuoka et al., 1997). Moreover, mutations in subunit a reduced inhibition by bafilomycin A (Wang et al., 2005); therefore, it seems possible that the sensitivity toward different inhibitors is influenced by the presence of different isoforms of subunit a.

V-ATPases have previously been detected both biochemically (Chanson and Taiz, 1985; Ali and Akazawa, 1986) and histochemically (Zhang et al., 1996; Kluge et al., 2004) in the plant Golgi apparatus, and the analysis of *Arabidopsis* mutants has shown that the V-ATPase is necessary for the structural integrity of Golgi stacks (Dettmer et al., 2005; Strompen et al., 2005). The fact that immunogold labeling of VHA-a1–GFP and VHA-E did not yield significant signals along Golgi stacks might simply reflect the fact that the pump density in the Golgi cisternae is below the detection limit. Mathematical modeling predicts that a small number of pumps would be sufficient to acidify certain compartments (Grabe and Oster, 2001); therefore, it seems possible that VHA-a1 is found throughout the secretory and endocytic pathways at levels below the detection limit.

Position of the TGN in the Plant Endosomal System

We used the styryl dye FM4-64, which is widely accepted as an endocytic tracer (Samaj et al., 2005), to determine the position of VHA-a1–GFP relative to the known markers of the endocytic pathway. To our surprise, we found that the first intracellular FM4-64 signals coincided with the TGN labeled by VHA-a1–GFP. The TGN has been defined as the clathrin-coated tubular network contained within the matrix of a Golgi stack (Staehelin and Moore, 1995), and the sorting of cargo destined either for vacuolar or secretory trafficking takes place in the TGN (Liu et al., 2002). However, there is evidence that the TGN may also be part of endocytic trafficking. Early ultrastructural work established the partially coated reticulum (Pesacreta and Lucas, 1985), a structure closely associated or identical with the TGN (Hillmer et al., 1988; Staehelin and Moore, 1995), as an early endosomal compartment (Tanchak et al., 1988). Endocytic cycling of plasma membrane proteins has been shown to be important for plant cell polarity and behavior (Geldner et al., 2003; Meckel et al., 2004), but structural and operational descriptions of plant endosomal compartments still need to be reconciled.

The molecular characterization of plant endosomes has relied to date on the analysis of the unique plant Rab GTPase, ARA6, and the *Arabidopsis* homolog of mammalian Rab5, ARA7 (Ueda et al., 2001). Transiently expressed ARA6 and ARA7 reside on distinct but partially overlapping populations of punctate structures, which have been shown by FM4-64 staining to represent endosomes (Ueda et al., 2004). In our hands, FM4-64 staining of the TGN occurred significantly faster than staining of either ARA6- or ARA7-positive compartments. The appearance of ARA7-positive endosomes is altered in cells lacking the ARF-GEF protein GNOM (Geldner et al., 2003), suggesting that GNOM-dependent recycling of plasma membrane proteins takes place in this compartment. If ARA7 indeed resides in a compartment equivalent to the recycling endosome (Ueda et al., 2004), this would only be stained after passage of FM4-64 through early or sorting endosomes. However, we cannot exclude the possibility that FM4-64 passes through ARA7 endosomes without accumulating to detectable levels before reaching the TGN, where it first becomes visible. The exact position of ARA7 in the endocytic pathway is still a matter of debate, as it has also been reported to be localized in the prevacuolar compartment (Lee et al., 2004) and to affect vacuolar trafficking (Kotzer et al., 2004). Assuming that endosomal maturation takes place, it will be of great interest to determine the relationship between the TGN and the endosomal compartments marked by the presence of Rab5-related proteins.

BFA has been instrumental in demonstrating the constitutive cycling of plant proteins between the plasma membrane and endosomal compartments (Geldner et al., 2001), but it

has been a matter of debate whether the BFA-induced vesicle agglomerations observed in *Arabidopsis* root cells are entirely Golgi-derived or, at least in part, endosomal (Wee et al., 1998; Nebenfuhr et al., 2002; Geldner et al., 2003; Grebe et al., 2003). We have shown here that the TGN is incorporated into BFA compartments, but our results also show that both views are not necessarily contradictory. However, our results indicate that costaining of intracellular signals with FM4-64 is not sufficient to demonstrate the cycling of plasma membrane proteins (Russinova et al., 2004). In the case of BRI1-GFP, intracellular fluorescence was greatly diminished after CHX treatment, indicating that it was largely derived from newly synthesized molecules in the TGN.

Whether endocytic and secretory cargos indeed merge in the TGN or the TGN has specialized subdomains that would allow the separation of both cargo types remains to be determined. For this purpose, it will be necessary to develop tools that can distinguish between newly synthesized and recycling plasma membrane proteins to be able to reliably trace the latter on their way into the cell.

V-ATPase Is Required for Secretory and Endocytic Trafficking

We have shown that ConcA leads to dramatic changes in Golgi and TGN morphology; therefore, the observed effects on secretory trafficking and vacuolar trafficking in tobacco cells (Matsuoka et al., 1997) are not surprising. Although we have provided only pharmacological evidence, our results are consistent with findings from other eukaryotes, and we have observed very similar effects on Golgi morphology in V-ATPase null mutants of *Arabidopsis* (Dettmer et al., 2005; Strompen et al., 2005).

How does V-ATPase inhibition lead to the observed effects on TGN and Golgi, and how does it interfere with BFA action? Similar effects on Golgi morphology have been described after treatment with the ionophore monensin, but in that case swelling and vacuolation can be ascribed to the osmotic water uptake caused by the exchange of cytoplasmic K^+ or Na^+ for luminal H^+ (Mollenhauer et al., 1990). Interestingly, it has been shown that membrane recruitment of components of the vesicle budding machinery, including ARFs, ARF-GEFs, and coat proteins, can depend on luminal acidification (Zeuzem et al., 1992; Aniento et al., 1996; Maranda et al., 2001). However, further studies of the role of the V-ATPase in the plant endomembrane system will also have to consider acidification-independent functions of V_0, as they have recently been described (Peters et al., 2001; Hiesinger et al., 2005). ConcA interferes with both endocytic and secretory trafficking and leads to the accumulation of cargo from both pathways in the ConcA-induced vesicle aggregates. Therefore, it could be argued that the proposed convergence of the two pathways is caused by the fusion of two otherwise independent compartments. However, the fact that nascent cell plates are heavily stained within 15 min after FM4-64 uptake provides strong evidence that the early convergence of endocytic and secretory trafficking is not an artifact caused by ConcA treatment.

Conclusions

We have determined the subcellular localization of the *Arabidopsis* VHA-a isoforms and have shown that the V-ATPase in the TGN is essential for endocytic and secretory trafficking. We propose that the TGN serves as a junction between early endocytic and secretory trafficking, and our results predict that the sorting of newly synthesized and internalized plasma membrane proteins may occur in the same compartment.

METHODS

Plant Materials and Growth Conditions

All plants used were *Arabidopsis thaliana* ecotype Col-0. Seedlings used for microscopy were grown on Murashige and Skoog (MS) medium + 1% sucrose at 22°C, with cycles of 16 h of light and 8 h of dark for 3 to 5 d.

Plasmid Constructs and Plant Transformation

For *VHA-a1* (At2g28520), a 10,421-bp *Cla*I fragment was isolated from BAC clone T17D12 and ligated into pBluescript II-KS+ (pBSII-KS+). A total of 1547 bp of the *VHA-a1* 3′ end was amplified by PCR from BAC T17D12, using the primers VHA-a1.XcmI.FOR and VHA-a1.KpnI-SpeI.REV (see Supplemental Table 1 online), and subcloned into pCR2.1-TOPO (Invitrogen). The subcloned PCR product was digested with *Kpn*2I-*Spe*I, and the resulting 414-bp fragment was ligated to the *Kpn*2I-*Spe*I–digested BAC fragment in pBSII-KS+. The genomic sequence, including a 1335-bp promoter and a 4670-bp coding sequence, was isolated via *Kpn*I from pBSII-KS+ and ligated into pGTkan. pGTkan is a derivate of pPZP212 (Hajdukiewicz et al., 1994) containing the GFP5(S65T) coding sequence and the pea (*Pisum sativum*) *rbcs* terminator.

For *VHA-a2* (At2g21410), a 7218-bp fragment of BAC clone F3K23 digested with *Kpn*I was ligated into pBSII-KS+. A total of 1792 bp of the *VHA-a2* 3′ end was amplified from BAC F3K23, using the primers VHA-a2-XbaI.FOR and VHA-a2-KpnI.REV, and subcloned into pCR2.1-TOPO. The subcloned PCR product was digested with *Xba*I and ligated to the *Xba*I-digested *Kpn*I fragment in pBSII-KS+. The genomic sequence, including a 3195-bp promoter and a 5436-bp coding sequence, of which 1775 bp was amplified by PCR, was isolated from pBSII-KS+ by partial digestion with *Kpn*I and ligated into pGTkan.

For *VHA-a3* (At4g39080), a 10,407-bp *Sac*I fragment of BAC clone F19H22 was ligated into pBSII-KS+. A total of 2126 bp of the *VHA-a3* 3′ end was amplified from BAC clone F19H22, using the primers VHA-a3-PstI.FOR and VHA-a3-KpnI.REV, and subcloned into pCR2.1-TOPO. The subcloned PCR product was digested with *Kpn*I-*Pst*I and ligated to the *Kpn*-*Pst*I–digested *Sac*I fragment in pBSII-KS+. The genomic sequence, comprising a 4146-bp promoter and a 5237-bp coding sequence, of which 2105 bp was amplified by PCR, was isolated from the pBSII-KS+ vector with *Sac*I-*Kpn*I and ligated into the pGTkan vector.

To exchange the VHA-a1 with the VHA-a2 3′ end, the genomic sequence of *VHA-a1* in pBSII-KS+ was digested with *Bam*HI, blunted using Accuprime Pfx DNA polymerase (Invitrogen), and finally cut with *Spe*I. This removes a 3498-bp fragment from the 3′ end. From the BAC clone F3K23, a 4083-bp PCR fragment was amplified with the primers a2-a1.for and a2-KpnISpeI.REV. The PCR product was cut with *Spe*I and phosphorylated with T4 PNK (Invitrogen) to allow blunt/*Spe*I ligation into pBSII-KS+ containing the 5′ end of VHA-a1. The 7428-bp chimeric fragment was isolated via partial *Kpn*I digestion and ligated into pGTkan. PCR amplifications were performed with Accuprime Pfx DNA polymerase (Invitrogen), and primers were purchased from Invitrogen or Metabion. All PCR-amplified fragments were controlled by sequencing performed by GATC.

The resulting binary plasmids were introduced into *Agrobacterium tumefaciens* strain GV3101:pMP90 and selected on 5 μg/mL rifampicin, 10 μg/mL gentamycin, and 100 μg/mL spectinomycin. Col-0 plants were transformed using standard procedures, and transgenic plants were selected on MS medium + 1% sucrose plates containing 50 μg/mL kanamycin.

Transient Expression of *Arabidopsis* Suspension Cultured Protoplasts

Polyethylene glycol–mediated transformation of *Arabidopsis* cell suspension protoplasts for transient coexpression of GFP- and RFP-fused proteins was performed with modifications to the protocol as described by Negrutiu et al. (1987).

RT-PCR

Total RNA was extracted from 5-d-old light-grown seedlings using the RNeasy plant mini kit (Qiagen) and used as a template for cDNA synthesis with Moloney murine leukemia virus reverse transcriptase (Fermentas) according to the manufacturer's instructions. The abundance of VHA-a1 and VHA-a1–GFP transcript levels was compared by PCR.

Immunoprecipitation

For total protein extracts, 4-d-old etiolated seedlings were ground in liquid nitrogen and resuspended in extraction buffer (50 mM Tris-HCl, pH 7.5, 150 mM NaCl, 0.5% Triton X-100, and 1× Complete protease inhibitor mix [Roche]). After incubation on ice for 30 min and centrifugation (300*g*, 4 min, 4°C), 0.8 mg of the supernatant was preincubated with 50 μL of protein A–agarose (Roche) (1 h, 4°C). After centrifugation, an aliquot of the supernatant was prepared for protein gel blot analysis (S1). The cleared supernatant was incubated with 1 μL of anti-GFP (Molecular Probes) or 1 μL of anti-hemagglutinin (Santa Cruz Biotechnology) antibody (1 h, 4°C). One hundred microliters of fresh protein A–agarose was added, and the incubation was continued for 3 h. The protein A beads were pelleted by centrifugation, and the supernatant was prepared for protein gel blot analysis (S2). The pellet was washed with 500 μL of 50 mM Tris-HCl, 150 mM NaCl, pH 7.5, and 10 mM NH_4HCO_3, pH 8, followed by boiling in 30 μL of sample buffer. Equal volumes of supernatant before (S1) and after (S2) precipitation were compared with the pellet fraction by protein gel blot analysis. We used the monoclonal antibody against V1 subunit VHA-A (Ward et al., 1992), horseradish peroxidase–conjugated rabbit α-mouse IgG antibodies, and the SuperSignal West Pico chemiluminescent (Pierce Perbio) for detection.

Fluorescent Markers

The coding sequence for SYP41-mRFP was amplified by PCR from a plasmid for transient expression (provided by T. Ueda) and cloned into the binary plant transformation vector pPZP312 carrying the 35S promoter and the rbcs terminator. pPZP312 is a derivative of the pPZP vectors carrying BASTA resistance under the control of the 5′ mas promoter and the 3′ mas terminator.

Transgenic plants expressing VHA-a1–GFP were transformed using standard procedures, and T1 seedlings were generated expressing ARA7-mRFP (Takano et al., 2005) or SYP41-mRFP and VHA-a1–GFP. The coding sequence of ARA7-GFP (Ueda et al., 2001) was excised from pBSII-KS+ and cloned into the binary vector pBINPLUS, and the resulting construct was transformed into wild-type plants using standard procedures. N-ST-YFP and ARA6-GFP have been described (Grebe et al., 2003).

Inhibitor Treatments and FM4-64 Staining

Three- to four-day-old seedlings were incubated in 1 mL of liquid medium (half-strength MS medium + 0.5% sucrose, pH 5.8) containing 50 μM BFA, 2 μM ConcA, or 50 μM CHX or combinations of these inhibitors. Endocytosis and colocalization studies were performed with 4 μM FM4-64. The seedlings were incubated with inhibitors and dye at room temperature for the indicated times. For time-dependent colocalization experiments, seedlings expressing VHA-a1–GFP, N-ST-YFP, ARA6-GFP, or ARA7-GFP were incubated for 3 min in medium containing FM4-64, then the seedlings were transferred to a microscope slide and imaged via CLSM. The following stock solutions were used: 50 mM BFA in DMSO: ethanol (1:1), 10 mM ConcA in DMSO, 20 mM wortmannin in DMSO, 50 mM CHX in DMSO, and 10 mM FM4-64 in DMSO. Control treatments were performed with equal amounts of the respective solvents.

Fluorescence Microscopy

Fluorescence microscopy was performed using a Leica TCS SP2 confocal laser-scanning microscope. All CLSM images were obtained using the Leica Confocal software and a 63× water-immersion objective. The excitation wavelength was 488 nm; emission was detected for GFP between 500 and 530 nm, for RFP between 565 and 600 nm, and for FM4-64 between 620 and 680 nm. Images were processed using Adobe Photoshop. Quantification of colocalization was performed by assessing the intensities of individual pixels within the images using the colocalization function of Metamorph Offline software (Universal Imaging).

Transmission Electron Microscopy

Immunogold labeling was performed on ultrathin thawed Tokuyasu cryosections of formaldehyde-fixed (8%, 3 h) and sucrose-infiltrated (2.1 M) root tips using rabbit anti-GFP serum (1:25; Abcam) or rabbit anti-VHA-E serum (1:500) (Betz and Dietz, 1991) and silver-enhanced (HQ Silver, 6 min; Nanoprobes) goat (Fab′) anti-rabbit IgG coupled to Nanogold (No. 2004; Nanoprobes). In parallel, GFP-labeled NST-GFP–expressing root cells were also labeled with a silver-enhanced (HQ Silver, 5 min) Quantum dot marker (goat $[Fab']_2$ anti-rabbit-IgG coupled to Qdot525 [1:20]; No. 1144-1; Tebu-lab). For structural analysis, root tips were either chemically fixed with 2.5% glutaraldehyde, 1% aqueous uranyl acetate, and 1% osmium tetroxide, dehydrated, and embedded in Epon or high-pressure frozen (Bal-Tec HPM 010; Balzers) in hexadecane (Merck Sharp and Dohme), freeze-substituted (72 h, −90°C; 8 h, −60°C; 8 h, −35°C; 4 h, 0°C) in acetone containing 2% osmium tetroxide and 0.5% uranyl acetate, washed at 0°C, and embedded in Epon.

Accession Numbers

Arabidopsis Genome Initiative numbers for the genes discussed in this article are as follows: VHA-a1, At2g28520; VHA-a2, At2g21410; VHA-a3, At4g39080.

Supplemental Data

The following materials are available in the online version of this article.

Supplemental Figure 1. VHA-a1–GFP Expression Levels and Integration into the V-ATPase Complex.

Supplemental Figure 2. Ubiquitous Expression of VHA-a Isoforms.

Supplemental Figure 3. Colocalization of SYP41-GFP and SYP41-mRFP.

Supplemental Figure 4. Line Scan Analysis of Colocalization.

Supplemental Figure 5. Transport of FM4-64 to the Tonoplast in Suspension Cells.

Supplemental Table 1. Sequences of Primers.

ACKNOWLEDGMENTS

We thank Felicity de Courcy, Claudia Oecking, Gerd Jürgens, and Niko Geldner for critical reading of the manuscript. We thank Pankash

Dhonukshe (Center for Plant Molecular Biology), Junpei Takano, Takashi Ueda (University of Tokyo), Masa Sato (Kyoto University), and Tomohiro Uemura (RIKEN) for sharing mRFP-tagged markers and Markus Grebe (Umea Plant Science Center) for providing GFP marker lines. We are grateful to Zhao-Xin Wang and Dagmar Ripper for excellent technical assistance. This work was supported by the Deutsche Forschungsgemeinschaft (SFB 446: A20, Z2).

Received September 13, 2005; revised December 30, 2005; accepted January 9, 2006; published February 3, 2006.

REFERENCES

Ali, S., and Akazawa, T. (1986). Association of the H^+-translocating ATPase in the Golgi membrane system from suspension-cultured cells of sycamore (*Acer pseudoplantanus* L.). Plant Physiol. **81,** 222–227.

Aniento, F., Gu, F., Parton, R.G., and Gruenberg, J. (1996). An endosomal beta COP is involved in the pH-dependent formation of transport vesicles destined for late endosomes. J. Cell Biol. **133,** 29–41.

Bassham, D.C., Sanderfoot, A.A., Kovaleva, V., Zheng, H., and Raikhel, N.V. (2000). AtVPS45 complex formation at the trans-Golgi network. Mol. Biol. Cell **11,** 2251–2265.

Bayer, M.J., Reese, C., Buhler, S., Peters, C., and Mayer, A. (2003). Vacuole membrane fusion: V0 functions after trans-SNARE pairing and is coupled to the Ca^{2+}-releasing channel. J. Cell Biol. **162,** 211–222.

Belanger, K.D., and Quatrano, R.S. (2000). Membrane recycling occurs during asymmetric tip growth and cell plate formation in *Fucus distichus* zygotes. Protoplasma **212,** 24–37.

Betz, M., and Dietz, K.J. (1991). Immunological characterization of two dominant tonoplast polypeptides. Plant Physiol. **97,** 1294–1301.

Bolte, S., Talbot, C., Boutte, Y., Catrice, O., Read, N.D., and Satiat-Jeunemaitre, B. (2004). FM-dyes as experimental probes for dissecting vesicle trafficking in living plant cells. J. Microsc. **214,** 159–173.

Campbell, R.E., Tour, O., Palmer, A.E., Steinbach, P.A., Baird, G.S., Zacharias, D.A., and Tsien, R.Y. (2002). A monomeric red fluorescent protein. Proc. Natl. Acad. Sci. USA **99,** 7877–7882.

Chanson, A., and Taiz, L. (1985). Evidence for an ATP-dependent proton pump on the Golgi of corn coleoptiles. Plant Physiol. **78,** 232–240.

Clague, M.J., Urbe, S., Aniento, F., and Gruenberg, J. (1994). Vacuolar ATPase activity is required for endosomal carrier vesicle formation. J. Biol. Chem. **269,** 21–24.

Dettmer, J., Schubert, D., Calvo-Weimar, O., Stierhof, Y.D., Schmidt, R., and Schumacher, K. (2005). Essential role of the V-ATPase in male gametophyte development. Plant J. **41,** 117–124.

Drose, S., Bindseil, K.U., Bowman, E.J., Siebers, A., Zeeck, A., and Altendorf, K. (1993). Inhibitory effect of modified bafilomycins and concanamycins on P- and V-type adenosinetriphosphatases. Biochemistry **32,** 3902–3906.

Forgac, M. (1999). Structure and properties of the clathrin-coated vesicle and yeast vacuolar V-ATPases. J. Bioenerg. Biomembr. **31,** 57–65.

Friedrichsen, D.M., Joazeiro, C.A., Li, J., Hunter, T., and Chory, J. (2000). Brassinosteroid-insensitive-1 is a ubiquitously expressed leucine-rich repeat receptor serine/threonine kinase. Plant Physiol. **123,** 1247–1256.

Geldner, N. (2004). The plant endosomal system—Its structure and role in signal transduction and plant development. Planta **219,** 547–560.

Geldner, N., Anders, N., Wolters, H., Keicher, J., Kornberger, W., Muller, P., Delbarre, A., Ueda, T., Nakano, A., and Jurgens, G. (2003). The Arabidopsis GNOM ARF-GEF mediates endosomal recycling, auxin transport, and auxin-dependent plant growth. Cell **112,** 219–230.

Geldner, N., Friml, J., Stierhof, Y.D., Jurgens, G., and Palme, K. (2001). Auxin transport inhibitors block PIN1 cycling and vesicle trafficking. Nature **413,** 425–428.

Grabe, M., and Oster, G. (2001). Regulation of organelle acidity. J. Gen. Physiol. **117,** 329–344.

Grebe, M., Xu, J., Mobius, W., Ueda, T., Nakano, A., Geuze, H.J., Rook, M.B., and Scheres, B. (2003). Arabidopsis sterol endocytosis involves actin-mediated trafficking via ARA6-positive early endosomes. Curr. Biol. **13,** 1378–1387.

Hajdukiewicz, P., Svab, Z., and Maliga, P. (1994). The small, versatile pPZP family of Agrobacterium binary vectors for plant transformation. Plant Mol. Biol. **25,** 989–994.

Herman, E.M., Li, X., Su, R.T., Larsen, P., Hsu, H., and Sze, H. (1994). Vacuolar-type H^+-ATPases are associated with the endoplasmic reticulum and provacuoles of root tip cells. Plant Physiol. **106,** 1313–1324.

Hiesinger, P.R., Fayyazuddin, A., Mehta, S.Q., Rosenmund, T., Schulze, K.L., Zhai, R.G., Verstreken, P., Cao, Y., Zhou, Y., Kunz, J., and Bellen, H.J. (2005). The V-ATPase V0 subunit a1 is required for a late step in synaptic vesicle exocytosis in Drosophila. Cell **121,** 607–620.

Hillmer, S., Freundt, H., and Robinson, D.G. (1988). The partially coated reticulum and its relationship to the Golgi apparatus in higher plant cells. Eur. J. Cell Biol. **47,** 206–212.

Huss, M., Ingenhorst, G., Konig, S., Gassel, M., Drose, S., Zeeck, A., Altendorf, K., and Wieczorek, H. (2002). Concanamycin A, the specific inhibitor of V-ATPases, binds to the V(o) subunit c. J. Biol. Chem. **277,** 40544–40548.

Iwaki, T., Goa, T., Tanaka, N., and Takegawa, K. (2004). Characterization of *Schizosaccharomyces pombe* mutants defective in vacuolar acidification and protein sorting. Mol. Genet. Genomics **271,** 197–207.

Kane, P.M. (2000). Regulation of V-ATPases by reversible disassembly. FEBS Lett. **469,** 137–141.

Kawasaki-Nishi, S., Bowers, K., Nishi, T., Forgac, M., and Stevens, T.H. (2001a). The amino-terminal domain of the vacuolar proton-translocating ATPase a subunit controls targeting and in vivo dissociation, and the carboxyl-terminal domain affects coupling of proton transport and ATP hydrolysis. J. Biol. Chem. **276,** 47411–47420.

Kawasaki-Nishi, S., Nishi, T., and Forgac, M. (2001b). Arg-735 of the 100-kDa subunit a of the yeast V-ATPase is essential for proton translocation. Proc. Natl. Acad. Sci. USA **98,** 12397–12402.

Kawasaki-Nishi, S., Nishi, T., and Forgac, M. (2001c). Yeast V-ATPase complexes containing different isoforms of the 100-kDa a-subunit differ in coupling efficiency and in vivo dissociation. J. Biol. Chem. **276,** 17941–17948.

Kinoshita, T., Cano-Delgado, A., Seto, H., Hiranuma, S., Fujioka, S., Yoshida, S., and Chory, J. (2005). Binding of brassinosteroids to the extracellular domain of plant receptor kinase BRI1. Nature **433,** 167–171.

Kluge, C., Lahr, J., Hanitzsch, M., Bolte, S., Golldack, D., and Dietz, K.J. (2003). New insight into the structure and regulation of the plant vacuolar H^+-ATPase. J. Bioenerg. Biomembr. **35,** 377–388.

Kluge, C., Seidel, T., Bolte, S., Sharma, S.S., Hanitzsch, M., Satiat-Jeunemaitre, B., Ross, J., Sauer, M., Golldack, D., and Dietz, K.J. (2004). Subcellular distribution of the V-ATPase complex in plant cells, and in vivo localisation of the 100 kDa subunit VHA-a within the complex. BMC Cell Biol. **5,** 29.

Kotzer, A.M., Brandizzi, F., Neumann, U., Paris, N., Moore, I., and Hawes, C. (2004). AtRabF2b (Ara7) acts on the vacuolar trafficking pathway in tobacco leaf epidermal cells. J. Cell Sci. **117,** 6377–6389.

Landolt-Marticorena, C., Williams, K.M., Correa, J., Chen, W., and Manolson, M.F. (2000). Evidence that the NH_2 terminus of Vph1p, an integral subunit of the V0 sector of the yeast V-ATPase, interacts directly with the Vma1p and Vma13p subunits of the V1 sector. J. Biol. Chem. **275,** 15449–15457.

Lee, G.J., Sohn, E.J., Lee, M.H., and Hwang, I. (2004). The Arabidopsis rab5 homologs rha1 and ara7 localize to the prevacuolar compartment. Plant Cell Physiol. **45,** 1211–1220.

Leng, X.H., Manolson, M.F., and Forgac, M. (1998). Function of the COOH-terminal domain of Vph1p in activity and assembly of the yeast V-ATPase. J. Biol. Chem. **273,** 6717–6723.

Leng, X.H., Nishi, T., and Forgac, M. (1999). Transmembrane topography of the 100-kDa a subunit (Vph1p) of the yeast vacuolar proton-translocating ATPase. J. Biol. Chem. **274,** 14655–14661.

Li, X., and Sze, H. (1999). A 100 kDa polypeptide associates with the V0 membrane sector but not with the active oat vacuolar H(+)-ATPase, suggesting a role in assembly. Plant J. **17,** 19–30.

Liu, T., Mirschberger, C., Chooback, L., Arana, Q., Dal Sacco, Z., MacWilliams, H., and Clarke, M. (2002). Altered expression of the 100 kDa subunit of the Dictyostelium vacuolar proton pump impairs enzyme assembly, endocytic function and cytosolic pH regulation. J. Cell Sci. **115,** 1907–1918.

Manolson, M.F., Proteau, D., Preston, R.A., Stenbit, A., Roberts, B.T., Hoyt, M.A., Preuss, D., Mulholland, J., Botstein, D., and Jones, E.W. (1992). The VPH1 gene encodes a 95-kDa integral membrane polypeptide required for in vivo assembly and activity of the yeast vacuolar H(+)-ATPase. J. Biol. Chem. **267,** 14294–14303.

Manolson, M.F., Wu, B., Proteau, D., Taillon, B.E., Roberts, B.T., Hoyt, M.A., and Jones, E.W. (1994). STV1 gene encodes functional homologue of 95-kDa yeast vacuolar H(+)-ATPase subunit Vph1p. J. Biol. Chem. **269,** 14064–14074.

Maranda, B., Brown, D., Bourgoin, S., Casanova, J.E., Vinay, P., Ausiello, D.A., and Marshansky, V. (2001). Intra-endosomal pH-sensitive recruitment of the Arf-nucleotide exchange factor ARNO and Arf6 from cytoplasm to proximal tubule endosomes. J. Biol. Chem. **276,** 18540–18550.

Matsuoka, K., Higuchi, T., Maeshima, M., and Nakamura, K. (1997). A vacuolar-type H^+-ATPase in a nonvacuolar organelle is required for the sorting of soluble vacuolar protein precursors in tobacco cells. Plant Cell **9,** 533–546.

Meckel, T., Hurst, A.C., Thiel, G., and Homann, U. (2004). Endocytosis against high turgor: Intact guard cells of *Vicia faba* constitutively endocytose fluorescently labelled plasma membrane and GFP-tagged K-channel KAT1. Plant J. **39,** 182–193.

Mollenhauer, H.H., Morre, D.J., and Rowe, L.D. (1990). Alteration of intracellular traffic by monensin: Mechanism, specificity and relationship to toxicity. Biochim. Biophys. Acta **1031,** 225–246.

Morel, N., Dedieu, J.C., and Philippe, J.M. (2003). Specific sorting of the a1 isoform of the V-H^+ATPase a subunit to nerve terminals where it associates with both synaptic vesicles and the presynaptic plasma membrane. J. Cell Sci. **116,** 4751–4762.

Nebenfuhr, A., Ritzenthaler, C., and Robinson, D.G. (2002). Brefeldin A: Deciphering an enigmatic inhibitor of secretion. Plant Physiol. **130,** 1102–1108.

Negrutiu, I., Shillito, R., Potrykus, I., Biasini, G., and Sala, F. (1987). Hybrid genes in the analysis of transformation conditions. Plant Mol. Biol. **8,** 363–373.

Nelson, N. (2003). A journey from mammals to yeast with vacuolar H^+-ATPase (V-ATPase). J. Bioenerg. Biomembr. **35,** 281–289.

Nishi, T., and Forgac, M. (2002). The vacuolar (H^+)-ATPases—Nature's most versatile proton pumps. Nat. Rev. Mol. Cell Biol. **3,** 94–103.

Oberbeck, K., Drucker, M., and Robinson, D. (1994). V-type ATPase and pyrophosphatase in endomembranes of maize roots. J. Exp. Bot. **45,** 235–244.

Padmanaban, S., Lin, X., Perera, I., Kawamura, Y., and Sze, H. (2004). Differential expression of vacuolar H^+-ATPase subunit c genes in tissues active in membrane trafficking and their roles in plant growth as revealed by RNAi. Plant Physiol. **134,** 1514–1526.

Parton, R.M., Fischer-Parton, S., Watahiki, M.K., and Trewavas, A.J. (2001). Dynamics of the apical vesicle accumulation and the rate of growth are related in individual pollen tubes. J. Cell Sci. **114,** 2685–2695.

Perzov, N., Padler-Karavani, V., Nelson, H., and Nelson, N. (2002). Characterization of yeast V-ATPase mutants lacking Vph1p or Stv1p and the effect on endocytosis. J. Exp. Biol. **205,** 1209–1219.

Pesacreta, T.C., and Lucas, W.C. (1985). Presence of a partially-coated reticulum in angiosperms. Protoplasma **125,** 173–184.

Peters, C., Bayer, M.J., Buhler, S., Andersen, J.S., Mann, M., and Mayer, A. (2001). Trans-complex formation by proteolipid channels in the terminal phase of membrane fusion. Nature **409,** 581–588.

Peyroche, A., Antonny, B., Robineau, S., Acker, J., Cherfils, J., and Jackson, C.L. (1999). Brefeldin A acts to stabilize an abortive ARF-GDP-Sec7 domain protein complex: Involvement of specific residues of the Sec7 domain. Mol. Cell **3,** 275–285.

Robineau, S., Chabre, M., and Antonny, B. (2000). Binding site of brefeldin A at the interface between the small G protein ADP-ribosylation factor 1 (ARF1) and the nucleotide-exchange factor Sec7 domain. Proc. Natl. Acad. Sci. USA **97,** 9913–9918.

Robinson, D.G., Albrecht, S., and Moriysu, Y. (2004). The V-ATPase inhibitors concanamycin A and bafilomycin A lead to Golgi swelling in tobacco BY-2 cells. Protoplasma **224,** 255–260.

Russinova, E., Borst, J.W., Kwaaitaal, M., Cano-Delgado, A., Yin, Y., Chory, J., and de Vries, S.C. (2004). Heterodimerization and endocytosis of Arabidopsis brassinosteroid receptors BRI1 and AtSERK3 (BAK1). Plant Cell **16,** 3216–3229.

Samaj, J., Read, N.D., Volkmann, D., Menzel, D., and Baluska, F. (2005). The endocytic network in plants. Trends Cell Biol. **15,** 425–433.

Sanderfoot, A.A., Kovaleva, V., Bassham, D.C., and Raikhel, N.V. (2001). Interactions between syntaxins identify at least five SNARE complexes within the Golgi/prevacuolar system of the Arabidopsis cell. Mol. Biol. Cell **12,** 3733–3743.

Schumacher, K., Vafeados, D., McCarthy, M., Sze, H., Wilkins, T., and Chory, J. (1999). The Arabidopsis det3 mutant reveals a central role for the vacuolar H(+)-ATPase in plant growth and development. Genes Dev. **13,** 3259–3270.

Schwacke, R., Schneider, A., van der Graaff, E., Fischer, K., Catoni, E., Desimone, M., Frommer, W.B., Flugge, U.I., and Kunze, R. (2003). ARAMEMNON, a novel database for Arabidopsis integral membrane proteins. Plant Physiol. **131,** 16–26.

Staehelin, L.A., and Moore, I. (1995). The plant Golgi apparatus. Annu. Rev. Plant Physiol. Plant Mol. Biol. **46,** 261–288.

Strompen, G., Dettmer, J., Stierhof, Y.D., Schumacher, K., Jurgens, G., and Mayer, U. (2005). Arabidopsis vacuolar H-ATPase subunit E isoform 1 is required for Golgi organization and vacuole function in embryogenesis. Plant J. **41,** 125–132.

Sze, H., Li, X., and Palmgren, M.G. (1999). Energization of plant cell membranes by H^+-pumping ATPases. Regulation and biosynthesis. Plant Cell **11,** 677–690.

Sze, H., Schumacher, K., Muller, M.L., Padmanaban, S., and Taiz, L. (2002). A simple nomenclature for a complex proton pump: VHA genes encode the vacuolar H(+)-ATPase. Trends Plant Sci. **7,** 157–161.

Takano, J., Miwa, K., Yuan, L., von Wiren, N., and Fujiwara, T. (2005). Endocytosis and degradation of BOR1, a boron transporter of *Arabidopsis thaliana*, regulated by boron availability. Proc. Natl. Acad. Sci. USA **102,** 12276–12281.

Tanchak, M.A., Rennie, P.J., and Fowke, L.C. (1988). Ultrastructure of the partially coated reticulum and dictyosomes during endocytosis by soybean protoplasts. Planta **175,** 433–441.

Tawfeek, H.A., and Abou-Samra, A.B. (2004). Important role for the V-type H(+)-ATPase and the Golgi apparatus in the recycling of PTH/PTHrP receptor. Am. J. Physiol. Endocrinol. Metab. **286,** E704–E710.

Toyomura, T., Oka, T., Yamaguchi, C., Wada, Y., and Futai, M. (2000). Three subunit a isoforms of mouse vacuolar H(+)-ATPase. Preferential expression of the a3 isoform during osteoclast differentiation. J. Biol. Chem. **275,** 8760–8765.

Ueda, T., Uemura, T., Sato, M.H., and Nakano, A. (2004). Functional differentiation of endosomes in Arabidopsis cells. Plant J. **40,** 783–789.

Ueda, T., Yamaguchi, M., Uchimiya, H., and Nakano, A. (2001). Ara6, a plant-unique novel type Rab GTPase, functions in the endocytic pathway of *Arabidopsis thaliana.* EMBO J. **20,** 4730–4741.

Uemura, T., Ueda, T., Ohniwa, R.L., Nakano, A., Takeyasu, K., and Sato, M.H. (2004). Systematic analysis of SNARE molecules in Arabidopsis: Dissection of the post-Golgi network in plant cells. Cell Struct. Funct. **29,** 49–65.

van Weert, A.W., Dunn, K.W., Gueze, H.J., Maxfield, F.R., and Stoorvogel, W. (1995). Transport from late endosomes to lysosomes, but not sorting of integral membrane proteins in endosomes, depends on the vacuolar proton pump. J. Cell Biol. **130,** 821–834.

Wang, Y., Inoue, T., and Forgac, M. (2005). Subunit a of the yeast V-ATPase participates in binding of bafilomycin. J. Biol. Chem. **280,** 40481–40488.

Ward, J.M., Reinders, A., Hsu, H., and Sze, H. (1992). Dissociation and reassembly of the vacuolar H^+-ATPase complex from oat roots. Plant Physiol. **99,** 161–169.

Wee, E.G., Sherrier, D.J., Prime, T.A., and Dupree, P. (1998). Targeting of active sialyltransferase to the plant Golgi apparatus. Plant Cell **10,** 1759–1768.

Zeuzem, S., Feick, P., Zimmermann, P., Haase, W., Kahn, R.A., and Schulz, I. (1992). Intravesicular acidification correlates with binding of ADP-ribosylation factor to microsomal membranes. Proc. Natl. Acad. Sci. USA **89,** 6619–6623.

Zhang, G.F., Driouich, A., and Staehelin, L.A. (1996). Monensin-induced redistribution of enzymes and products from Golgi stacks to swollen vesicles in plant cells. Eur. J. Cell Biol. **71,** 332–340.